The effect of particle shape on the packed bed effective thermal conductivity based on DEM with polyhedral particles on the GPU

Govender Nicolin, Cleary Paul W., Kiani-Oshtorjani Mehran, Wilke Daniel N., Wu Chuan-Yu, Kureck Hermann

DOI: 10.1016/j.ces.2020.115584

The effect of particle shape on the packed bed effective thermal conductivity based on DEM with polyhedral particles on the GPU

Nicolin Govender[1], Paul W Cleary [2], Mehran Kiani-Oshtorjani[3], Daniel N. Wilke[4], Chuan-Yu Wu[1], Hermann Kureck[5]

[1]Department of Chemical and Process Engineering, University of Surrey, Guildford, GU2 7XH, United Kingdom

[2]CSIRO Data61, Clayton, Victoria, 3168, Australia

[3]Department of Energy Technology, Lappeenranta University of Technology, Skinnarilankatu 34, 53850, Finland

[4]Department of Mechanical and Aeronautical Engineering, University of Pretoria, South Africa

[5]Research Center Pharmaceutical Engineering, GmbH, Graz, Austria

Abstract

Granular material (GM) is the second most manipulated substance in the world and is present in most industries either as raw materials or finished products. Often the temperature of the granular material needs to be manipulated for example in the case of heating iron ore to induce a phase change or to be kept within a certain temperature range in the case of pharmaceutical powders and food products. Thus a detailed understanding of how heat is transferred in granular materials is essential. The most feasible numerical approach to study heat transfer in granular materials is using the discrete element method (DEM), where each particle is explicitly modeled. In terms of conductive heat transfer particle shape can be expected to have a significant effect on the heating of granular materials, due to the nature of the grain to grain contacts and packing topology which control the heat flow paths and the rate that heat is conducted along these. This paper considers the effect of particle shape on heat conduction in thermally simple or low Biot number granular materials using a polyhedral particle representation. The volume based contact model for granular heat conduction is firstly verified against the analytical solution for solid heat conduction as well as experiment with cubic particles. The resulting model is then used to study the effect of particle shape on the effective thermal conductivity (ETC) and heat distribution within packed stationary beds. It was found that for irregularly shaped (polyhedral) particles the ETC does not have a linear relationship with the packing density as found in previous studies with spherical and ellipsoidal shaped particles. Rather that there is an exponential dependence on the micro-structural quantities of contact area and isotropy, with non-homogeneity in the packing density resulting in complex conduction paths and dead zones affecting conduction thru the bed.

1 Introduction

Heat transfer in granular media (GM) is almost as ubiquitous in nature as GM itself, being second only to water as the most manipulated substance on the planet [1]. Heat affects numerous processes that include catalyst reactors [2], energy storage, food processing, calciners and kilns. Some particle or inter-particle properties can significantly change over moderate temperature ranges, and can directly influence inter-particle flow and heat generation, which in turn affects granular advective heat transfer and heat energy in the system. For example, the influence of friction on heat transfer in hopper discharge of spherical particles [3], rotary calciners using a spherical particle system [4, 5, 6], experimental investigations into rotary drums [7], thermo-mechanical analysis of nuclear pebble failure [8], heat transfer in dense fluid-particle systems using parallelized compute [9] have been studied. Other parameters that influence percolation, elutration, agglomeration and flow-induced or transport mechanisms [10, 11] may also significantly affect granular advective heat transfer. Hence, computational approaches have been developed [12, 13, 14, 15] to improve the prediction of granular dynamics. These include taking into account microscopic behavior at the particle scale and improved modeling of advective heat transfer and energy transfer to heat energy. Some particle properties may change as a direct result of temperature, e.g. thermal expansion. The increase of

a material's volume due to an increase in temperature has been studied for 2D discs [16], and for more general spherical particle systems [17], to determine effective thermal expansion coefficients for granular packings.

In a granular system, a number of heat transfer mechanisms are responsible for transferring heat to, from and between particles. These include heat conduction within particles, heat conduction through the solid-solid interface (conductance between particles), radiative transfer between particles and either other particles or the environment. In addition, heat can be conducted from the surrounding fluids (gas or liquid) to the particles, where the fluids can be transported by natural convection, forced convection and advection with different temperatures. In addition, granular advection result due to the motion of the particles. Radiation transfers energy between particles through void spaces [18], only becoming important when temperatures are at least several hundred degrees, with sufficiently large inter-particle voids [19, 18]. Convection is strongly limited by the low permeability of the porous media until temperature gradients are sufficiently high to overcome the strong flow resistance. Consequently, conduction is the dominant heat transfer mechanism in granular materials at low to moderate temperatures. Conduction can be considered thermally simple with a uniform temperature field inside particles if their Biot number is less than 0.1 in which case particle to particle temperature variations control the overall conductive heat transfer. This study is focused on conductance between low Biot number polyhedral particles at lower temperatures allowing other transfer mechanisms of radiation and convection to be omitted.

Generally, granular media have thermal conductivities that are orders of magnitude lower than for solids made of the same material, resulting in a relatively low effective thermal conductivity (ETC) that is dependent on the nature of the particle packing. The ETC of a packed bed depends on a number of parameters including the solid volume fraction (SVF) [20], the particle thermal conductivity [21], contact pressure, particle surface roughness [22], stiffness, translucency affecting absorption and scattering [23], particle shape [24, 25], size of the particles and how they are packed [26, 27, 20]. Polamuri et al. [20] demonstrated that Bruggeman's equation for ETC is within 3% - 13% for mono-dispersed spherical particles in a regular packing. Perfect mono-dispersed spheres in a regular packing significantly simplifies the spatial void fraction description, as it is constant over the packing, resulting in a uniform ETC. The ETC for mono-dispersed spherical steel particles, with diameters between 1 mm and 12 mm, were found to be between 100 and 160 times smaller than for solid steel. Experimental work by [28] indicated that the ETC of binary particles particle systems are higher than unary particle systems, due to the poor conductvity of air between particles. For binary packings, ETC is at its maximum when the void fraction is at its minimum. For the same volume fraction, a higher fraction of smaller particles result in a lower ETC due to an increase in the number of small to small particle contacts that effectively increases the thermal resistance along a thermal transmission path. Lee et al. [29] demonstrated that for binary particle systems consisting of non-homogenous materials, large insulating particles enhance thermal conduction compared to smaller insulating particles, due to larger insulating particles improving the interconnectivity of thermally conductive particles for the same volume fractions. The reason being that larger insulating particles are more spatially localized, reducing the chances of interrupting a conductive path, when compared to smaller insulating particles that are spatially more dispersed. The effective thermal conductivity in a packed bed has contributions due to conduction, convection and radiation, i.e. a contribution for each mode of heat transfer. Wang et al. [30] showed the role that gas convection plays in enhancing ETC for random spherical packings. Wang et al. [18] also showed that at elevated temperatures (> 1000 K) for stagnant flows the increase in ETC with temperature was mainly due to radiation, which tends to be more pronounced for large void fractions.

In the absence of convective and radiative heat transfer, the ETC in spherical particle systems is largely influenced by the characteristics of i) contact domains, ii) contact positions, iii) contact angles and iv) contact stresses [31, 32, 26, 33]. Changes in particle shape significantly affects all four characteristics leading to vastly different force chain networks that in turn affect the ETC as shown experimentally by Huchet et al. [25]. Although, the experiments provide a reliable packed bed ETC, they cannot be utilized to provide insight into the mechanistic connections between particle shape as characterised by micro-mechanical quantities such as the contact area, contact number, packed bed topology, heat flow paths and the resulting rate of heat transfer. In addition, empirical relations predicting the ETC have been derived based on these experiments but are limited to the paraamter ranges over which the experiments were conducted [21, 34, 22, 28, 20]. Therefore, simulations are a valuable tool to provide insight and understanding of the principles governing the ETC variation in packed beds. Unfortunately, modeling of thermal behaviour of granular aassemblies has to-date largely been dominated by investigation of circular 2D [35, 26, 36]. A limited number of studies have considered non-spherical particle shapes such as cubes to thermally analyse granular systems [37], with some being limited to 2D modelling assumptions [38]. This paper considers the effect of polyhedral particle shape represenatons on heat conduction in thermally simple or low Biot number granular packings.

1.1 Numerical Modeling

Thermal analysis of problems involving particles are often resolved using multiscale methods, which aim to extract predictive macroscopic properties by resolving the geometry and physics of an underlying microstructure [39]. The two main approaches to bridge the length scales are namely homogenization and coarse graining [40]. Homogenization averages properties over a micro-scale structure to recover macroscopc properties [24, 41, 19, 27], while (ii) coarse graining recovers the emergent behaviour across length scales through statistical and thermodynamical principles [40, 42]. Mesh-based continuum approaches such as the finite element method (FEM) [43], and finite volume method (FVM) [44], can be easily applied to estimate temperatures within irregularly shaped solids or in solids with non-uniform thermal properties. Energy conservation is reformulated into an integral form that is then solved in the strong or weak form by discretization resulting in a solution that satisfiesthe energy conservation equation globally. Although the governing equations and operations are much easier to discretize using the finite difference method (FDM) [45], their form in generalized coordinates are not. The FEM and FVM allows for the formulation of the problem from a conservation viewpoint, which FDM does not, giving FEM and FVM more explicit control over which quantities are enforced exactly and which ones approximately. All three approaches were originally designed and are well suited for heat transfer within single bodies. In a multi-body context, both for static and dynamic cases, complications arise for all three approaches, requiring contact to be resolved in order to obtain an effective contact area required to estimate conductance between bodies.

This allows the particle system to be treated numerically as a porous medium, which is popular when the effective macroscopic properties of the particle system can estimated from a detailed FEM or FVM thermal analysis [31]. The high computational efficiency of this approach makes it desirable when considering large granular assemblies. On the downside this approach is not well suited to accommodating particle level changes. Multi-scale FEM approaches resolve these particle scale changes by solving a micro-scale model at each finite element integration point, which comes at a significant compuational cost [46]. Meshless continuum methods such as the Lattice-Boltzmann Method (LBM) [47] and Smoothed Particle Hydrodynamics (SPH) [48], have mainly been applied to single particle systems or two-dimensional multiple particle systems.

In contrast, discrete approaches allow large number of particles and attempt to represent these particles individually using simplified models. Numerous approaches have been proposed that include thermal network models (TNM) [35], lattice element method (LEM) [49], parallel column models [50], and discrete element method (DEM) [37] to resolve thermal problems for granular assemblies. TMN and LEM, can loosely be viewed as generalizations of the FDM, in which each particle is modeled as an isothermal sphere. Contact pairs are modeled by an equivalent thermal resistance pipe, reducing the thermal equations of the whole system to that of a corresponding thermal resistance/conduction network. TNM and LEM, lack a rigorous theoretical foundation to determine thermal parameters. DEM in turn has proven to be extremely useful to estimate ETC in granular assemblies [37], and shown to even recover FDM results for single particle internal conduction [36]. However, DEM is computationally demanding, which consequently has seen limited applications mainly restricted to spherical particle systems [35, 26, 36].

Attempts to alleviate the computational demands of DEM include derivation of simpler models from DEM information such as discrete thermal element model (DTEM) [31], multi-sphere unit cell model [51] or combined FEM-DEM [52]. These simplifications may encounter difficulties or lose their computational advantages when considering dynamic applications of particle systems that flow. As an alternative to simplifying DEM models, DEM can be better aligned with compute devices. Performing DEM on graphical processing units (GPU) can improve computing times by orders of magnitude. A simplified isothermal DEM model allows for effective exploitation of multi-GPU compute without creating significant implementation drawbacks. However, a potential disadvantage of such a simplified model is that it is only valid for particle systems with Biot numbers $<< 1$ for which the internal heat transfer can be ignored since the temperature is fairly uniform inside the particles allowing for a "lumped" capacitance model to be assumed. Particle systems with higher Biot numbers require the internal thermal gradient over the particle to be resolved to maintain accurate approximations. Witt et al. [6] presented a thermal DEM method that included a one-dimensional variation of temperature within the particles which allows the method to be used for higher Biot number (insulating or larger particles). This method can be used in two and three dimensions and for dynamic (flow) problems but is limited to spherical particles as the internal one-dimensional approximation of the temperature field is only valid for spherical particles. Recently, [53]have used finite discrete element method (FDEM) to study intra-particle heat transfer in granular assemblies allowing for complex temperature fields to be resolved within complex shaped multi-bodied contact problems. While this does extend FEM beyond static problems, the size of the systems that can be analyzed are still limited to a few thousand with fairly long run times. Recent progress has been made using FDEM to model both fluid flow and heat transport [54], which again is limited to a few particles.

The majority of work in DEM thus far has been for packed bed problems supported by experimental studies ranging from loose [55, 56] to dense packings [57] [58], with the aim of characterizing heat flow through the granular beds. The modeling of thermal behaviour of granular assemblies are largely dominated by circular 2D [52], or spherical 3D particle systems [35, 26, 36]. A limited number of studies have considered non-spherical particle shapes to thermally analyse granular systems [37], with some being limited to 2D studies [38]. However, for real granular systems the particle shapes can be irregular and complex, which is distinct from the ideal spherical assumptions. As demonstrated experimentally, a dominant characteristic of granular assemblies for non-spherical, non-uniform and irregular particles is that the packing density as well as contact network varies which significantly affect the conduction of heat through a packing. Thermal conductance laws for discrete element models are mainly limited to spherical particle systems [59]. Only a limited number of studies have investigated non-spherical particle shapes using FDEM [60] to derive empirical relationships for the effective thermal conductivity [59].

This paper aims to explore the effect of particle shape on thermal conduction by approximating the contact area between particles using the volume overlap method [61]. To the best of the authors knowledge this is the first study to resolve the contact area between polyhedral particles to estimate the effective flux area that is known to drive conductance. Additionally, there are no closed form relationships that relate the overlapping volume of two contacting polyhedral particles to their thermal conductivity.

2 Computational Implementation

A caveat of DEM simulations is that tens millions of particles with process times in the order of minutes are typically required for the simulation of industrial problems, which is beyond the computational capability of current computers. Consider Figure 1 which depicts various particle shape approximations typically used in DEM. The spherical approximation Figure 1(a) is the most commonly used shape with the majority of conductivity studies to date having been performed using spheres with intangible modifications such as rolling friction to account for a departure from sphericity [62, 63]. This approach is limited as the relationship of rolling friction to particle shape is usually unknown requiring extensive characterization that diminishes the predictive ability of these models. Studies that considered particle shape usually limit themselves to ellipsoids Figure 1(c) [64], multi-sphere approximations [65], as depicted in 1(d) as depicted in Figure 1(d). A polyhedral shape representation is able to capture the particle angularity and aspect ratio as required with such a particle shown in Figure 1(e).

Collision detection between polyhedral particles is the most time consuming part of a DEM simulation. In Blaze-DEM [66, 67, 68] contact is split over three phases each with increasing computational cost. Contact between particles is first detected using an efficient strategy during the "broad phase" identifying potential contact pairs which are resolved during a computationally more demanding narrow phase to establish whether two particles are actually in contact and if so to compute the resulting force direction and magnitude can be computed. The broad phase for spherical and polyhedral shaped particles uses a hashing strategy such as Morton codes or spatial decomposition such as Bounding Volume Hierarchy (BVH). Identified contact particle groups are then directly resolved in a narrow phase for spherical particles to establish contact pairs and ultimately contact measures to calculate force directions and magnitudes. In turn, for convex polyhedral particles the broad phase is followed by an intermediate phase using some bounding primitive to detect contact more accurately than the broad-phase with a much cheaper query than a full contact check. This is followed by a narrow phase to establish contact pairs and ultimately contact measures to calculate force directions and magnitudes.

These forces can be estimated in various ways, that include estimating the penetration distance [69, 70, 71], in vertex-face and edge-edge contact. Alternatively, the forces can be estimated from the overlapping volume [69, 72, 73], which is the measure computed accurately in Blaze-DEM on the GPU (which is used here) that is significantly harder than finding the overlap distance. The benefit being that the overlapping volume allows for both the direction and magnitude to be resolved using an energy-conserving contact interaction scheme [61]. This approach also provides us with accurate surface contact area as well as the exposed surface area of the particle which is required for heat transfer.

To compute the overlap volume, consider the intersection of two polyhedral cubes as depicted in Figures 2(a). It is important to note that the intersection volume between two intersecting polyhedra is given by the convex hull formed using the vertices at the intersections between the polyhedral edges and faces. The first step is to find the intersecting vertices as depicted in Figure 2(b), after which we define the faces that form the convex hull of the overlap volume in Figure 2(c). The surfaces of this volume are formed by the external face of one polyhedra with the internal faces within the other polyhedra. Once the surfaces have been identified the resultant force can

be computed by integrating over the surfaces as depicted in Figure 2(d) with the contact area being the common face(s) shared between the polyhedra.

Lastly, two additional contact volume properties that need to be computed are the contact Volume V and the COM of the contact volume as these will be required to resolve the elastic contact force. Since, both V and COM changes between contacts it is necessary to compute them efficiently on the GPU. The divergence theorem

$$\iiint_V (\nabla \cdot F)\, V = \oiint_{S(V)} \oiint F \cdot \mathbf{S}, \tag{1}$$

allows us to transform the volume integral of an object with volume V into the surface integral around the boundary surface $S(V)$ of the volume with outward-pointing normal. This can be done by appropriately choosing any vector field $\mathbf{F}(x_1, x_2, x_3)$ that has a divergence of 1 i.e. $\nabla \cdot \mathbf{F} = 1$. This then gives the volume

$$\oiint_{S(V)} \oiint F \cdot \mathbf{S} = \iiint_V V = V, \tag{2}$$

as a surface integral. As an alternative, the contact volume can be computed by sub-dividing the intersection volume into tetrahedra for which efficient closed form expressions exist in computing volumetric and inertial properties [74]. Once, these quantities have been computed the reaction force direction is calculated as

$$\mathbf{n}_i^f = \frac{\int_A \mathbf{n}_i^A ds}{|\int_A n_i^A ds|} = \frac{1}{\sum_j A^j} \sum_j A^j \mathbf{n}_i^{A_j}, \tag{3}$$

which acts on particle i as shown respectively in Figures 2(d) for the two particles. Here, the direction of the reaction forces are respectively indicated by the solid lines (red and black). In addition, the computed reaction force acts through the COM of the overlap volume, while the magnitude of the reaction force in turn is proportional to the volume V of the contact volume. For particle i, the elastic force associated with contact volume V, follows the following constitutive relationship:

$$\mathbf{F}^i = kV\mathbf{n}_i^f, \tag{4}$$

where k is a numerical stiffness coefficient. Additional forces including a viscous damping force that depends on the relative velocity and rotation between the particles as well as the tangential forces complete the contact forces on the particle as depcited in Figure 3.

2.1 Heat Transfer Models

The heat flux between contacting particles i and j is given by Fourier's law as:

$$Q_{ij} = H_c(\triangle T_c) \tag{5}$$

where $\triangle T_c$ is the apparent temperature difference between particles and H_c is the heat conductance coefficient. The parameter $H_c = \frac{\lambda_p A}{\gamma_c}$ is a measure of the thermal resistance of material, where λ_p is the material thermal conductivity, A is the cross-section area, and γ_c is the distance through which the temperature gradient applies (we denote it as γ_c to distinguish it from the continuous media). As there is no temperature gradient inside individual particles, determining $\gamma_c = \Delta x$ is not straightforward. However, from the analytical solution for the spherical particles, we know $H_c = 2\lambda_p\sqrt{A}$ [5, 4]. Any general relation for H_c for non-spherical shapes should asymptotically approach this as the particle shape approaches spherical. Consequently we assume the general form H_c as:

$$H_c = \alpha\lambda_p\sqrt{A_c} \tag{6}$$

where A_c is the contact area based on the penetration distance for spheres or the polygonal contact area. While $\alpha = 2$ in the case of spherical particles [5, 4] for polyhedra there exists no general geometric description of the irregularly shaped contact area, hence this factor will need to be determined via experimental means. Figure 4 illustrates a polyhedron with three contacting neighbours each having a contact area $\boldsymbol{A}$that is calculated from the surfaces of the overlap polyhedron that is determined in Figure 2(d). Addtionally the contact angle θ that is required for subsquent istropy calculations is defined as the vector between the target particle center and the center of the overlap polyhedron relative to the positive vertical axis.

The resultant temperature change of particle i can be expressed as

$$T_i^{n+1} - T_i^n = \frac{\sum_j Q_{ij}}{m_i C_p^i} \triangle t \tag{7}$$

where C_p^i is the specific heat of the particle i, subscript j stands for the contacts that particle i has, and superscripts $n+1$ and n are for the new and previous time steps, respectively. The main assumption of the model is that thermal conduction inside a particle is fast enough that the temperature over a particle can be assumed uniform, meaning that the thermal gradient over a particle is negligible since (Biot < 0.1) [16].

3 Determination of the heat transfer coefficient and model validation

We firstly aim to determine the value of the conduction coefficient α for perfectly contacting polyhedral particles using the well-known example of heat transfer in a solid for which there is an analytical solution (time dependent heat equation). The material used is aluminum having a conductivity of 240 $\mathrm{W.m^{-1}K^{-1}}$ and heat capacity of 921J.kg^{-1}.K^{-1}. An advantage of using polyhedra is that we can create a totally solid packing of cubic particles, which in effect is a discretisation of a continuous solid (25 cm x 30 cm x 25 cm) as depicted in Figure 5 (a). In this case, all cubes are face contacting with an area of 0.25 cm^2 and edge length of 0.50 cm. The side walls are adiabatic with the top and bottom surfaces held at 100 and 0 °C respectively as shown in Figure 5 (b). We use the fact that at steady state the ETC of the packed bed will be equal to the material thermal conductivity thus allowing us to determine the relationship between α and ETC. Figure 5 (b) contains a plot of the ETC as a function of α, we notice a linear relation with $\alpha = 0.86$ corresponding to the thermal conductivity of aluminum.

Now that we have determined the value of α for this scenario we can verify the code by comparing the solution using the heat equation to the simulated solution as a function of time. Figure 6 (a) shows the evolution of the temperature in the bed at various vertical positions over time with Figure 6 (b) depicting the spatial distribution of temperature at steady state. We observe a good agreement at the various time intervals indicating that both the contact method used and the equation for heat conduction is correct. Furthermore we have demonstrated that the unknown parameter α in the thermal resistance of contact (Equation 5) can be calibrated to a target value for the material under investigation.

3.1 Experimental Conditions

Having verified the model for a perfect contact (conduction) scenario, we aim to validate the code experimentally. We now need to determine the conduction coefficient α for non-perfectly contacting particles. The experimental setup to perform the conductance heat transfer is outlined in Figure 7. An inductive heat source was used to heat and maintain oil at 70 ± 1°C. The value of 70 °C was chosen to avoid radiative effects, vapor forming as well as the maximum output of the source. An iron bar of dimension 250mm x 50 mm x 10 mm weighing 760 grams was suspended on insulated wooden supports. Particles are made of milled aluminum having dimensions of 19 mm square with a thickness of 3 mm with the outside surfaces at which contacts occur been polished as depicted in Figure 7 (b). The particles were maintained at 24.3 °C within 0.1 °C using a thermal bath to ensure uniform initial conditions before being placed on the heated iron bar. The dimensions of the iron bar is selected to act as a reservoir requiring 337 J to increase the temperature by 1°C, while 2.7 J of energy would increase the temperature of an aluminum particle by 1°C. Thereby, increasing the energy of a single particle from bath temperature to the iron bar temperature would at most result in 0.3°C change in temperature of the iron bar. A FLIR thermal camera was used to experimentally measure the surface temperature fields of each particle over time. The FLIR thermal camera requires a reflected background correction to compensate for environmental radiation. Before each experiment the background temperature was compensated for and the emissivity of the FLIR thermal camera was set for aluminum. A single particle was placed with its 3 mm face on the hot plate, supported by a thermally insulated bracket with subsequent particles placed on top of the first particle with a weight of 1 kg placed on top to ensure consistent contact.

3.2 Numerical Conditions

The linear-spring dashpot model described in Equation (4) was used with a normal stiffness of $\mathrm{k} = 1000 \frac{\mathrm{N}}{m}$, time-step of 1×10^{-5} and a coefficient of restitution (COR) of 0.40. The thermal properties of the material are the same as the preceding section. While Equation 6 concerns itself with perfect conduction in reality for contacting bodies we

have thermal resistance at the contact area due to imperfections in surface finish and environmental contaminants. Thus we need to firstly determine the factor by which the previously determined conduction coefficient α needs to be modified to account for this. As in the previous case we choose a single data point at which to calibrate α_1 to match the experimental temperature of 36.5 ± 0.52^{o}C at 10s. The value of α_1 between the source and particle was calculated to be 0.20, so thermal resistance between the particle and iron plate reduces conductance by around 4x (changing the weight on top beyond 1 kg had no effect). In order to determine α_2 for contact between particles we follow the same procedure this time matching the temperature of the top particle at 30 s which was found to be $29.6 \pm 0.18^{o}C$. The value α_2 was calculated to be 0.08, hence the thermal resistance between particles reduces conductance by around 10x. Unlike thermal conductivity for which there exists a substantial library of values for various conditions, the data for thermal resistance is sparse existing for just a few conditions and materials. Therefore these results should be viewed in the context of the current study as a means of validating the heat transfer model for polyhedral particles rather than an exercise on determining the general thermal resistance for contacting polyhedra.

3.3 Validation with Experiment

We now investigate the predictability of the code by comparing the simulated results to that of experiment for single particle on a heated surface contact as shown in Figure 8(a) with Figure 8(b) showing the corresponding images captured by the thermal camera. The temperatures contained in the image correspond to the heat probes on the camera and are labeled as spot 1-3. As can be seen in Figure 8(a) there is a good match between the experiment and numerical results with the relative error been less than one percent. Finally we compare the results for the case of two contacting particles with the bottom particle on the heated surface. Figure 9(a) depicts the experimental and simulation results, we again see a good match for both particles temperatures indicating that we are able to predict the correct thermal behavior with Figure 9(b) show the images captured by the thermal camera, note that spot 3 is the temperature of the air. We see that there is little change in the ambient temperature showing that other heating mechanisms have negligible effects at the temperature range of the experiment.

4 Numerical study on the ETC of a packed bed

Having verified and validated the contact model and conductance laws, we now proceed to study the effect of particle shape on the effective thermal conductivity (ETC) of packed beds. While there have been previous studies on the ETC of packed beds for spherical particles this is the first study, to the best of the authors knowledge, to consider polyhedral particles. The rectangular ($25 \times 25 \times 30$ cm^3) packed bed under investigation is depicted in Figure 10(a). The bed is generated by releasing particles with the same initial velocity of 1 $^{m}/_{\mathrm{s}}$ from a height of 50 cm with a uniform random orientation allowing them to settle down under gravity. Packed beds are generated for several particle shapes as illustrated in Figure 10(b) were (1-5) are convex while (6) is a non-convex shape that is used to demonstrate the flexibility of the code. The common geometric feature between particles was choose to be the volume (0.125 cm^3) which has been used in previous study in-order to gain shape effects between dissimilar geometric representations. It is also should be noted that the convex shapes (items 1-4) have a similar aspect ratio while the HexP (item 5) has an elongated width resulting in an aspect ratio of (1:8). The physical and numerical parameters of the particles are tabulated in Table 1. In order to ensure the same height of the packed bed for all shapes, filling was performed starting from above the 30 cm target height and any particles that were above this height after packing was completed were removed

The temperature of particles contacting the top boundary (30 cm) is held constant at 100^{o}C (T_{top}) while those at bottom boundary (0 cm) is held constant at 0^{o}C (T_{bot}). The initial temperature of the bed is set to 0^{o}C with the vertical walls been adiabatic in order to ensure the imposed temperature gradient is only in the vertical direction. Once a thermally steady state condition is reached, we have:

$$\sum_{j} Q_{ij} = 0 \tag{8}$$

where the sum is over all particles in the system. However, the total heat fluxes to and from the top and bottom plates are not zero. We denote the total heat flux through the top plate as Q. The heat flux through the bottom plate is necessarily -Q since the system is at thermal steady state. As a result, the effective thermal conductivity of packed bed is calculated as:

$$\lambda_{eff} = \frac{Q}{A}\frac{\triangle y}{\triangle T} \tag{9}$$

where $\Delta y = 30\,cm$ is the height, $A = 625\,\mathrm{cm}^2$ the cross section area of packed bed, $\triangle T = 100^{\circ}\mathrm{C}$ the temperature gradient between the plates and Q the calculated heat flux from Equation (5).

Macroscopic Analysis The numerical parameters used for the simulations here is the same as in Section 3.2 , a representative volume from the middle of the bed was extracted to provide a qualitative view of the packing structure as depicted in Figure 11. Table 2 lists the calculated ETC, packing density, average contact area as well as various geometric identifiers for each shape. We firstly notice that the shape with the highest solid volume fraction (SVF) namely cubes does not have the largest ETC, in fact there is no relationship between the SVF and ETC. This is significant as previous studies involving spheres have found a linear relationship between the SVF and ETC, furthermore higher average contact areas do not necessarily yield the largest ETC values either. The non-convex shape exhibits the most striking deviation from the current understanding of ETC from packed beds of spheres, in that it has one of the smallest average contact areas (similar to spheres) yet it has an ETC that is 68% higher. Equally baffling is that the HexP shape which is convex, has one of the largest average contact areas but has the lowest ETC of the polyhedral shapes. These findings demonstrate the traditional macroscopic properties of packed beds namely SVF and contact area are insufficient to characterize the thermal conductive properties of packed beds consisting of polyhedral shapes.

Analysis of Packing Structure To explore the packing structure the distribution of contact angles (defined in Figure 2) relative to the vertical direction as well as the variation of contact area along the vertical axis of the bed is shown in Figure 12 (a). From Figure 12 (a) we firstly notice that the HexP has a peak close around 12 degrees indicating a strong ordering in the vertical direction with a lack of horizontal contacts as they have packed with the long axis in the horizontal direction (Figure 11(e)). Secondly we notice that the CrossP particle which is non-convex, does not have a strong peak indicating its contacts are fairly uniform resulting in the highest isotropy of all polyhedra but still less than spheres owing to a lack of vertical contacts (< 30 degrees). The remaining polyhedra have similar distributions peaking between 40 and 45 degrees, with the cube particle having a secondary waeker peaks occurring at 0 and 90 degrees respectively. The corresponding contact isotropy weighted by the contact area is listed in Table 2 and provides a single measure of the results depicted in Figure 12.

Gravity and particle shape are the two main factors that determine the distribution of contact pressures over the height of a packed bed. Since all particle shapes have the same mass, any variations in the resulting distributions may be attributed to particle shape. Figure 12 (b) shows how the contact area varies as a function of height. While we observe a trend of stronger contacts at the bottom, the variation with height in the beds differs for the various polyhedra shapes. Spherical particles have the smallest variation implying that the average contact area is the most similar throughout the depth of the bed. This is consistent with the findings of previous studies using spheres [35, 26, 36] where the bed is assumed to be homogeneous. However, for the case of polyhedra we see that there is a significant variation through the depth of the bed with the largest variation belonging to the HexP particle. This result demonstrates that the assumption of homogeneity in packed beds is not valid for polyhedral particle shapes.

The contact network is illustrated in Figure 13 where the colors indicate the relative normalized contact area over all cases while the thickness indicates the strength of the contact relative to that particular shapes contacts. We firstly notice that the most uniform and co-incidentally dense contact networks belong to the Cubic and TTet shapes respectively which both have the highest ETC values while the BiLuna and Sphenome shapes have a less dense network with weaker contacts. The HexP shape on the other-hand has strong contacts which take the form of vertical "zig zags", which lends support to the assertion of islands forming due to vertical stacking as supported by 12 (a) which significantly reduces the ETC. Finally we observe that for the spherical particles the network is very ordered with contacts typical of a Hexagonal Close Packing (HCP) as expected for mono-sized spheres.

Next we quantify the microstructural properties presented in Figure 12 for convex polyhedra by finding correlations to the ETC. Figure 14(a) shows the ETC as a function of the contact area, we notice a linear relationship with contact area, except for the HexP shape. However the HexP shape is the most dis-similar of convex polyhedra due to its high aspect ratio resulting in large flat faces along its principal axis which is indicative that the aspect ratio of the particle also has an effect on the packing micro structure. Figure 14 (b) shows the ETC as a function of contact angle isotropy θ (Figure 2) weighted by the contact area. We observe that all convex shapes now fit an exponential curve (fitting parameters in the text box within the figure), which illustrates that both the contact area and the orientation of the contacts is needed to provide a more holistic correlation.

Distribution of Heat within the bed While the ETC characterizes heat conduction in a packed bed at steady state it is also important to understand transient behavior. Figure 15 (b) depicts the time to ready steady state (here termed the relaxation time) for each convex polyhedral shape. The Sphenome and HexP with the lowest ETC values require a longer time to reach steady state reflecting the slower rate of heat conduction through the particle networks. The slower conduction rate thru the contact network is a result of having lower isotropy and weaker contacts than the other convex polyhedra as shown in Figure 12 (a) where the peak of the Sphenome shape is shifted from the others and is closer to the HexP shape. This lack of isotropy and the preference to have stronger contacts in the vertical direction results in the aniostropic distribution of heat in the bed in line with the findings of the micro-structural analysis that contact area and isotropic dictates the flow of heat in the bed. Figure 15(b) shows the plot of ETC as a function of the relaxation time for all convex shapes. The relationship is exponential (fitting parameters in the text box within the figure) which is in contrast to the linear relationship found for packed beds composed of spherical particles [35, 26, 36].

The steady state vertical temperature profile of the stationary packed bed is depicted in Figure 16 (a) for convex polyhedra shapes. For a uniform continuous material this temperature profile is linear as shown by the solid line in the plot. However this is not the case for a granular material due to the complex network for conduction which is anisotropic containing dead ends and bottle necks depending on the local micro-structure of the packing. Thus in Figure 6 we observe that the temperature profiles mimic parabolas with the turning point occurring at the vertical distance at which the mean temperature occurs. The HexP and Sphenome shapes which have the lowest ETC values have the largest deviation from a linear temperature distribution at steady state, with the curvature becoming less prominent for shapes having larger ETC values. This parabolic behavior is attributed to the non-uniformity of contacts resulting from variations on the local packing structure which can be seen in Figure 16 (b). In Figure 16 (b) we observe that at the top the packing is the least dense resulting in a lower conductivity while the packing in middle is more dense with a plateau resulting in a higher conductivity and finally the bottom having the highest packing density and conductivity. The TTet shape has the most uniform packing density and thus requires the shortest time to reach steady state. Although the TTet shape does not have the highest packing density, it has the least variation in packing density and contact area, coincidentally it also has the largest contact area and is the most isotropic. The HexP shape with has the lowest packing density and largest variations of both packing density and contact area, has the lowest ETC, longest relaxation time and is the least isotropic.

Finally Figure 17 depicts the temperature profile graphically where particles are colored by their temperatures at steady state. We notice that the Cubic and TTet shapes have the most uniform spacing of color bands with the temperature at the middle been almost the mean of the two boundary temperatures. While the other convex shapes have a much lower mean temperature thus resulting in a larger spectrum of colder bands from the bottom.

5 Conclusion

This paper demonstrated that by calculating the intersection volume between contacting polyhedra an accurate estimate of the contact area, for which there are no closed-form solutions can be obtained. It was then demonstrated that this estimates area can be used in the well known heat conduction equations for spherical particles by calibrating the heat transfer coefficient using theoretical or experimental data. The code was then validated against experiment using the calibrated coefficient values, demonstrating the predictability of the model used in the code. This is important as there are currently no models for the conduction of heat between polyhedral particles having a uniform temperature (no gradient). In addition, the volume overlap method proved suitable for both convex and non-convex shaped polyhedral particles. In total, seven particle shapes were considered, five convex polyhedra which are the focus of this study, one non-convex polyhedron used to demonstrate the flexibility of the code as well as a sphere which is used as the baseline particle in this study.

It was found that the relationship of linear scaling between ETC and packing density present for spherical particles does not hold for convex polyhedral shapes. The importance of this finding is that it eludes to the fact that we cannot readily use simple laboratory scale experiments which provide a measure of the bulk packing density to make predictions when dealing with polyhedral particles, thus making simulation the most viable tool for the understanding of thermal conductivity within packed beds.

The key finding of this study is that the micro-structural quantities of contact area and contact angle isotropy are required to characterize polyhedra packed beds rather than the bulk packing density. We found an exponential relationship between the ETC and contact angle isotropy (weighted by the contact area) for the convex shapes used in this study. This finding is supported by following observations:

1. Large variations in the packing density over the height of the bed effects the conduction networks resulting on deadzones (islands) and hotspots.

2. Shapes with the largest variations in per particle contact area had the lowest ETC values as well as requiring the longest to reach steady state.

3. Shapes with larger contact isotropy have higher ETC values.

Thus it can be concluded that particle shape significantly influences micro-mechnical topology and force chain variations, which in turn effects the thermal conductivity of the static packed bed. The ETC was observed to vary by 500% from the baseline spherical particle system with the time to reach steady state been two times less for the most conductive polyhedral case and 1.5 times larger in the case of the least conductive polyhedral case. These findings are also in contrast to the previously reported linear relationship with the packing density found for ellipsoidal shaped particles which are non-spherical. This demonstrates that the key aspect of irregularly shaped particles in reality contacting at a surface rather than at single points which is the case for spheres and ellipsoids significantly alters the thermal conductive behavior of the bed by causing variations in the micro-mechanical topography.

Acknowledgments

This work was supported by the MARIE Sklodowska-CURIE Individual Fellowships with acronym DECRON, funded through the People Programme (MARIE Sklodowska-CURIE Actions) of the European Union's H2020 under REA grant agreement No. 747963. We gratefully acknowledge the support of the NVIDIA Corporation with the donation of the Titan V GPU used for this research.

Figures

List of Figures

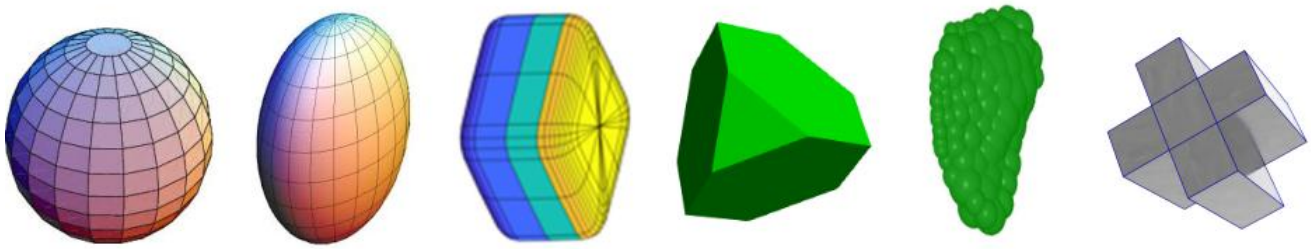

(a) (b) (c) (d) (e) (f)

Figure 1: Illustration of common shape representations in DEM (a) sphere, (b) ellipsoid, (c) superquadric, (d) convex polyhedra , (e) multi-sphere (compound of (a)) and (f) non-convex polyhedra (compound of (d)).

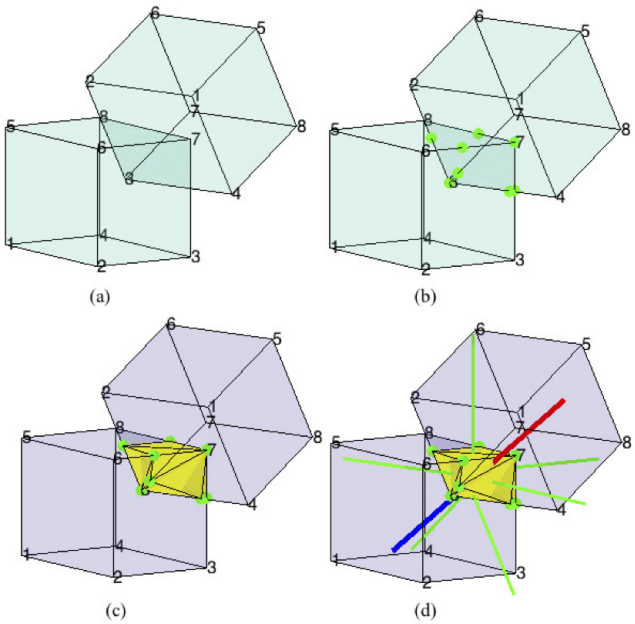

Figure 2: Contact resolution (a) between two intersection polyhedra by resolving the (b) contact points from which the (c) convex hull is constructed to compute the contact volume and (d) contact normals.

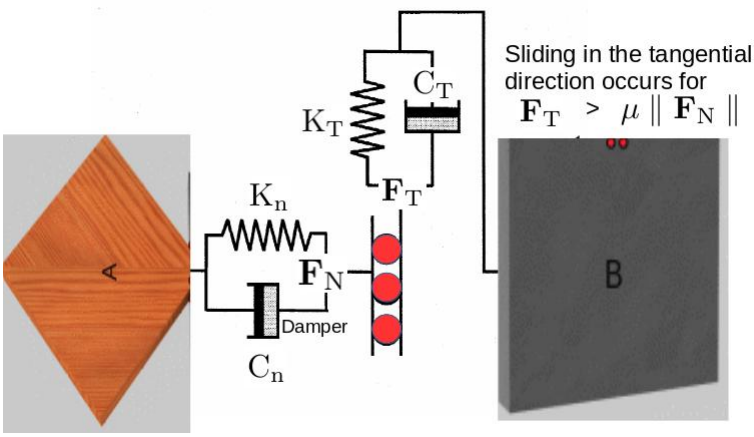

Figure 3: Normal and tangential contact force models represented by a spring dashpot system.

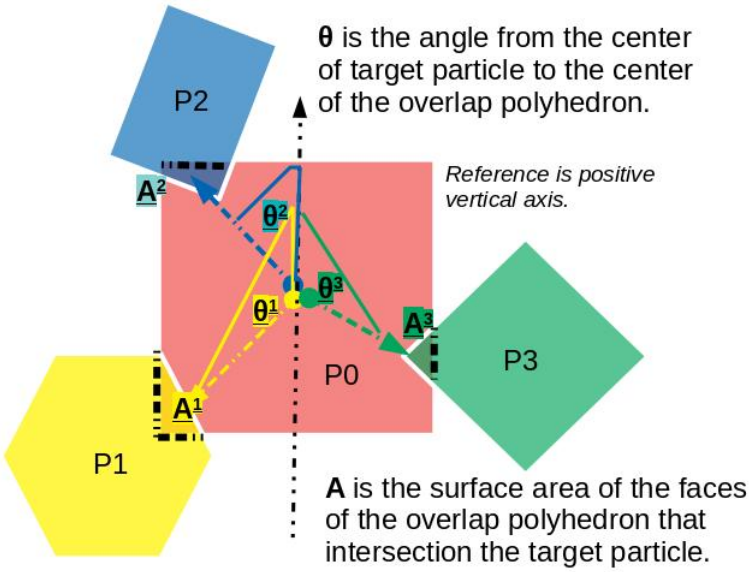

Figure 4: Two dimensional sketch of contact angle θ and contact area $\boldsymbol{A}$ between contacting particles.

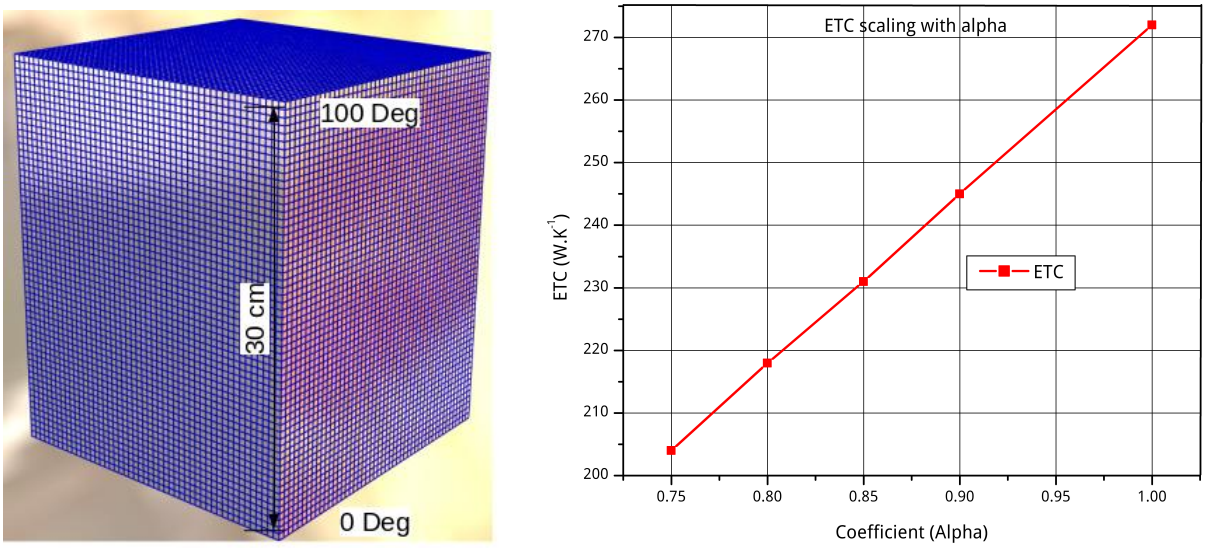

(a) (b)

Figure 5: (a) Solid composed of 144060 tightly packed cubic (0.25 cm) particles and (b) plot of ETC vs α for the tightly packed particles setup.

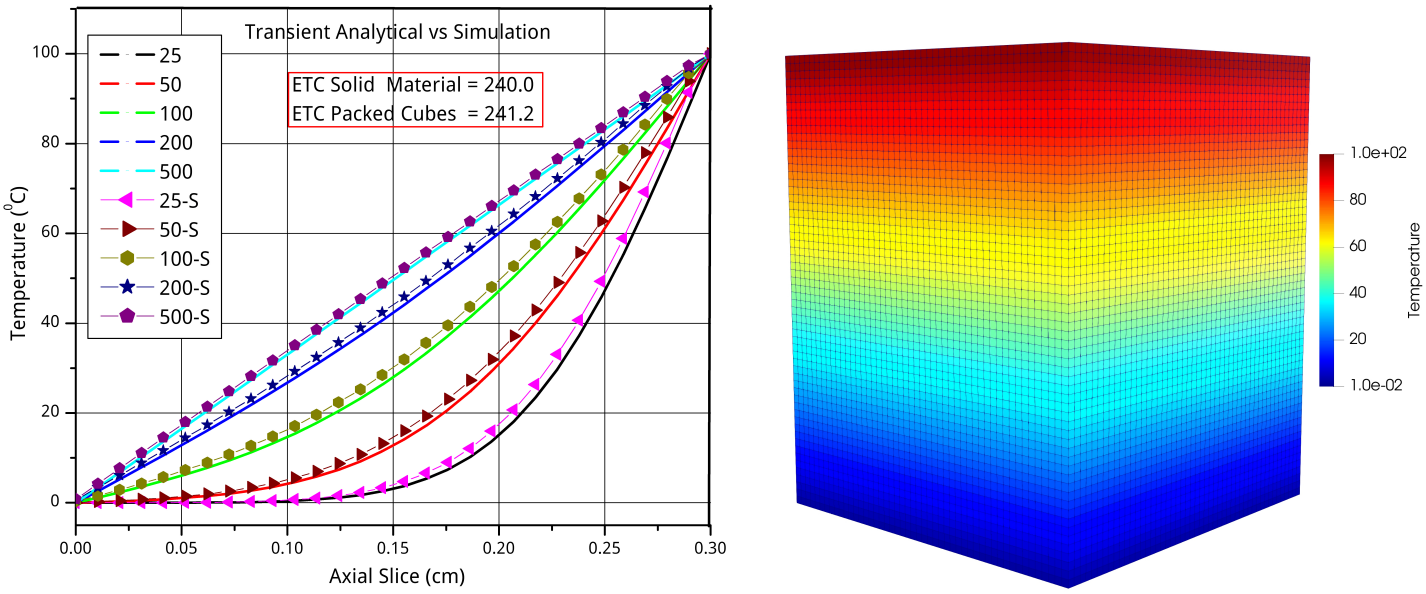

(a) (b)

Figure 6: (a) Temperature distribution over vertical slices (1 cm) and (b) simulation steady state of packed cubic particles at 500s .

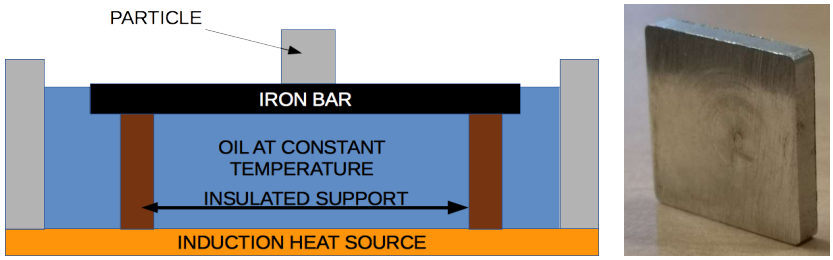

(a) (b)

Figure 7: (a) Schematic of the experimental setup and (b) aluminum square particle with milled finish used in the experiment.

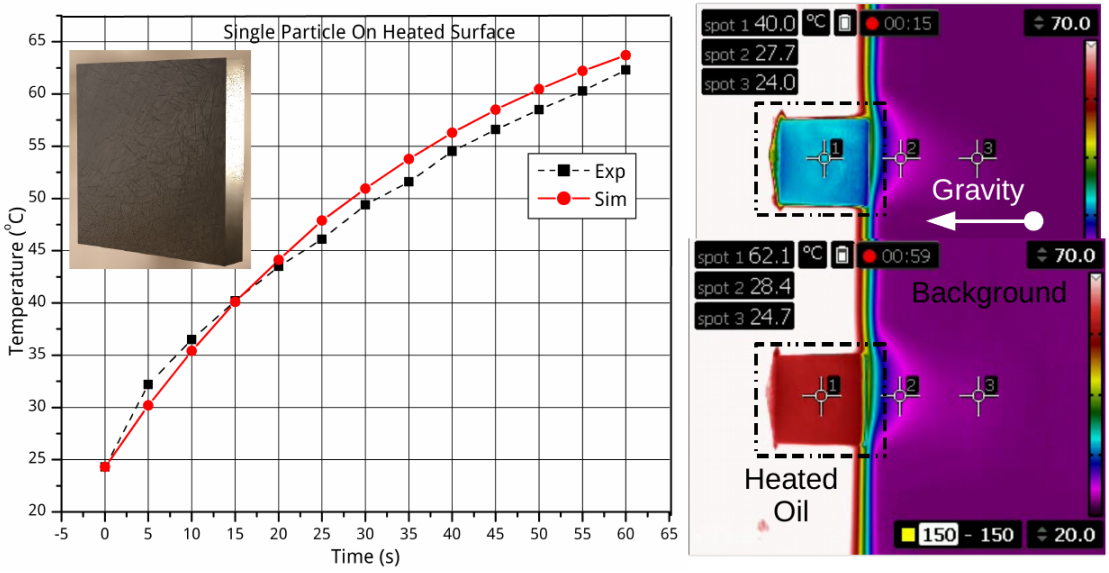

(a) (b)

Figure 8: (a) Experimental and simulation plot of temperature for a single cube on a constant (71 deg) temperature source and (b) the corresponding thermal camera captured image showing heating uniformity as well as heat sensor location and values.

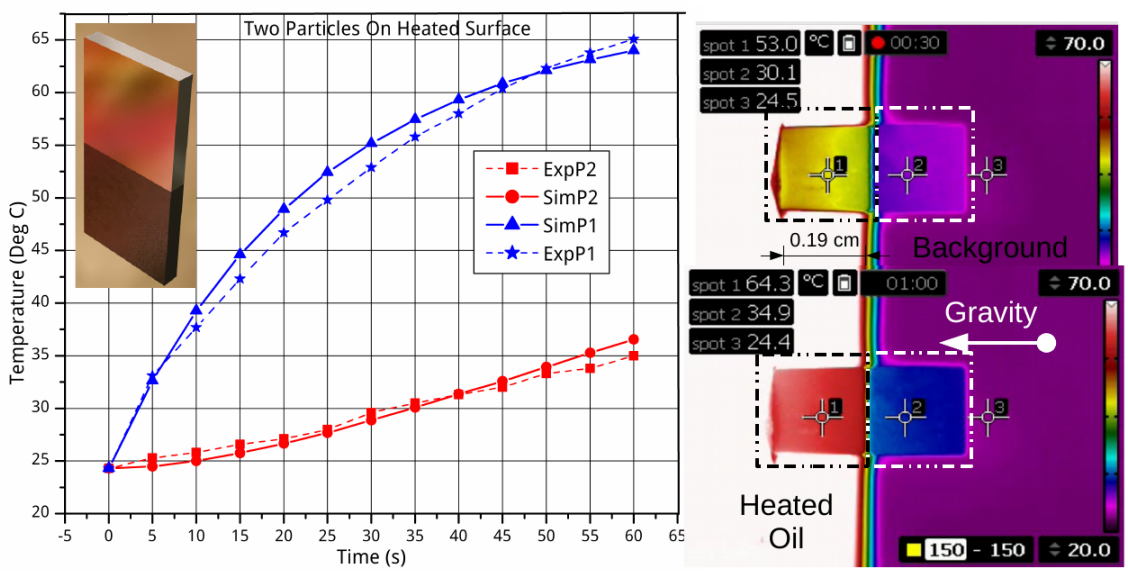

(a) (b)

Figure 9: (a) Experimental and simulation plot of temperature for a single cube on a constant (71 deg) temperature source and (b) he corresponding thermal camera captured image showing heating uniformity as well as heat sensor location and values.

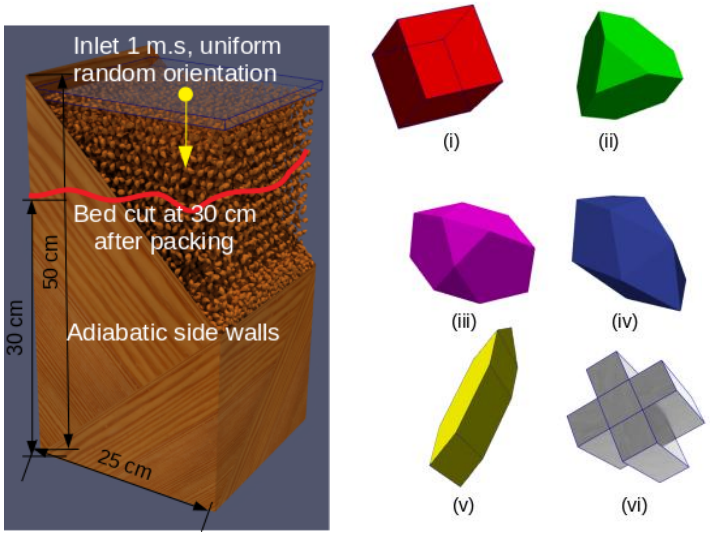

(a) (b)

Figure 10: (a) packed bed schematic illustrating filling and (b) particles shapes used in the simulation (i=Cube, ii=TTET, iii=BiLuna, iv=Sphenome, v=HexP and vi=CrossP).

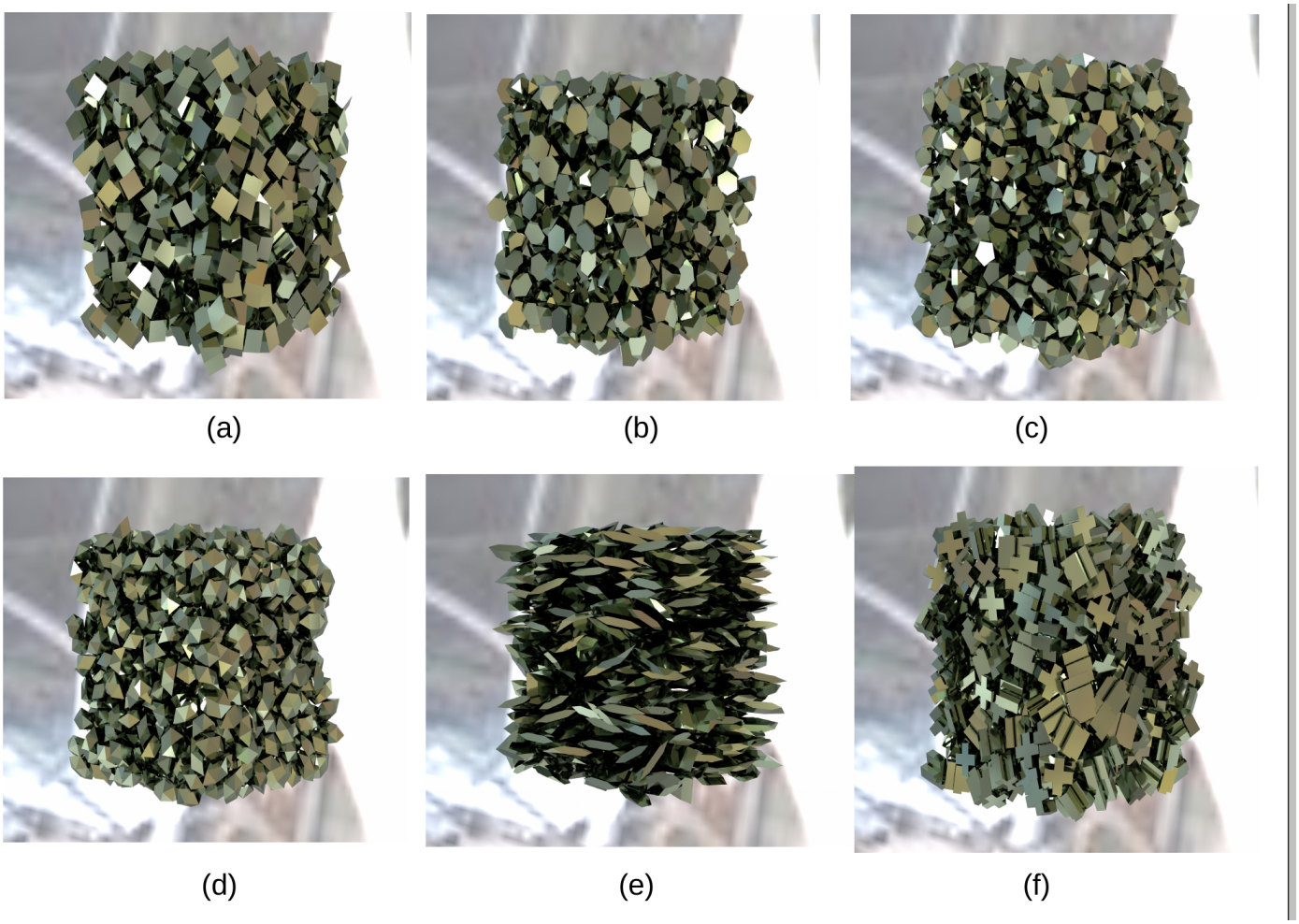

Figure 11: Packed state of particles in a 5 cm cubic region extracted from the middle of the bed (a) cubes, (b) truncated tetrahedron, (c) bilunabirotunda, (d) sphenomegacorona , (e) flattened augmented hexagonal prism and (f) non-convex cross prism.

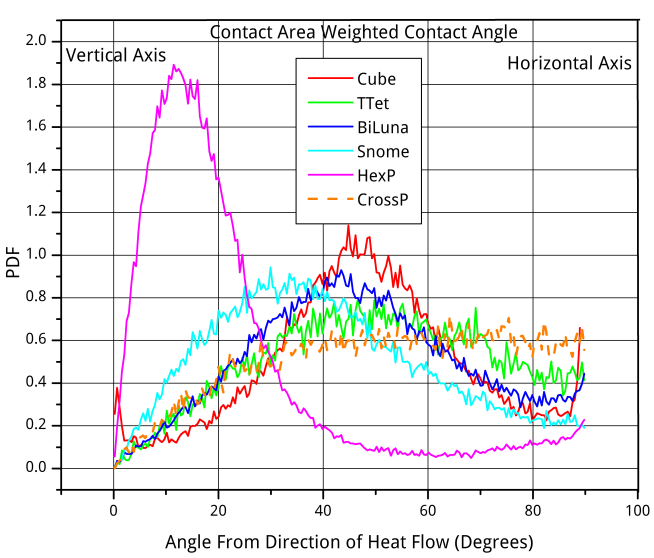

(a)

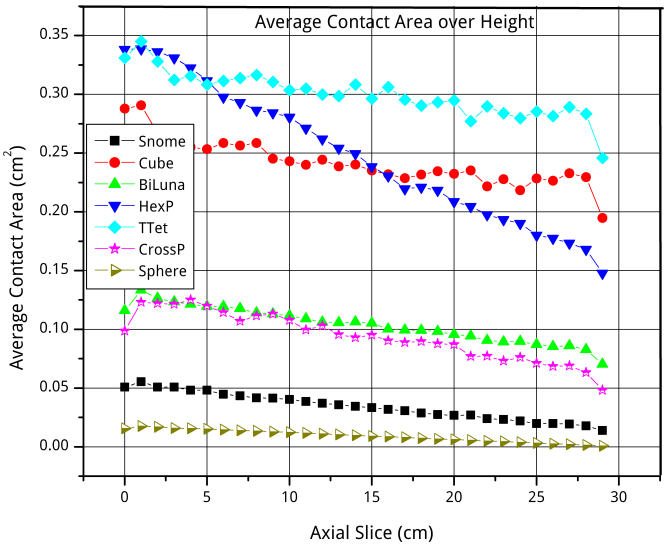

(b)

Figure 12: (a) contact angle relative to vertical direction and (b) average contact area over the height of the bed .

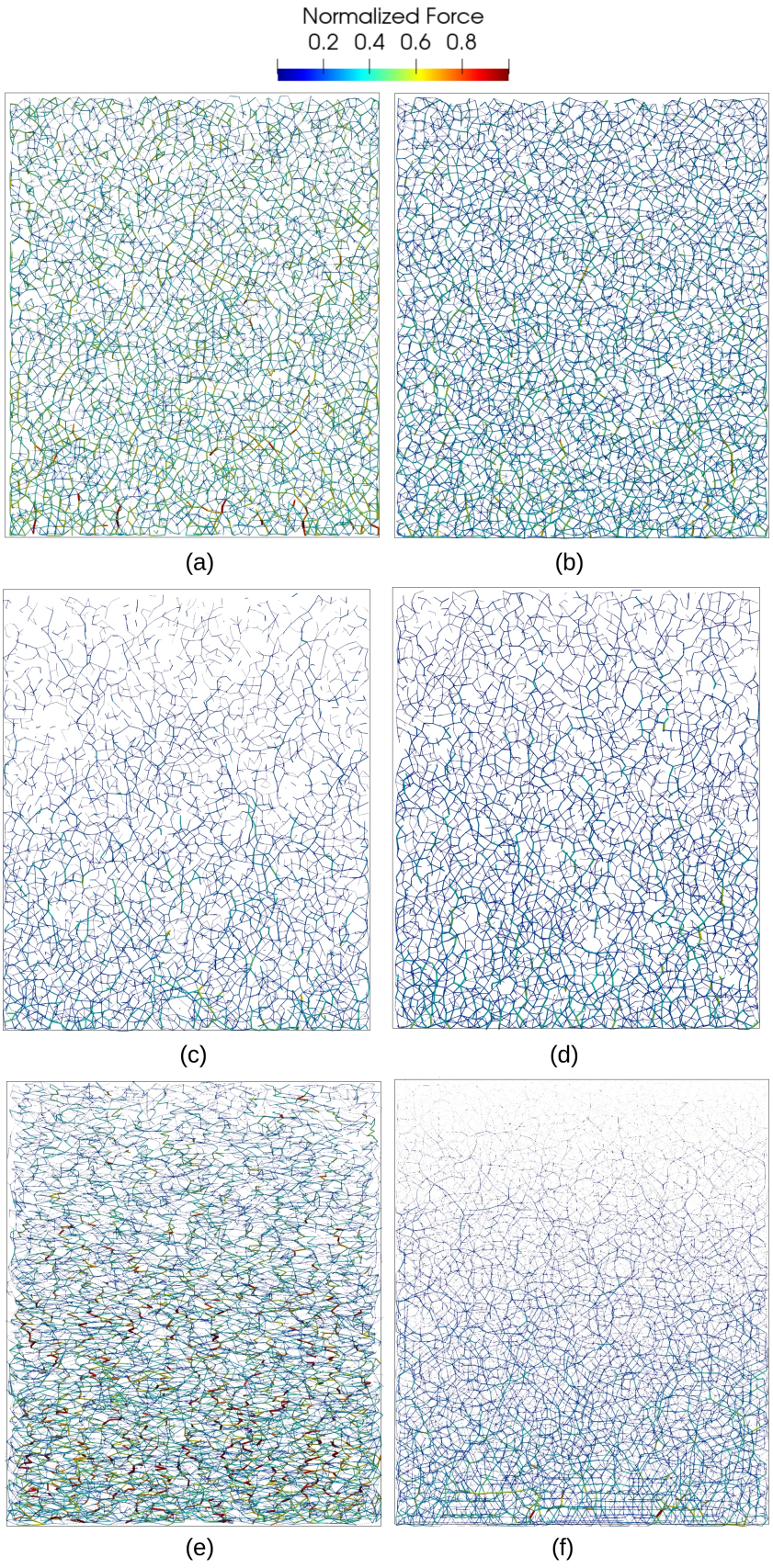

Figure 13: Normalized force chain network for (a) cubic, (b) truncated tetrahedron, (c) bilunabirotunda, (d) sphenomegacorona , (e) flattened augmented hexagonal prism and (f) spherical particle shapes

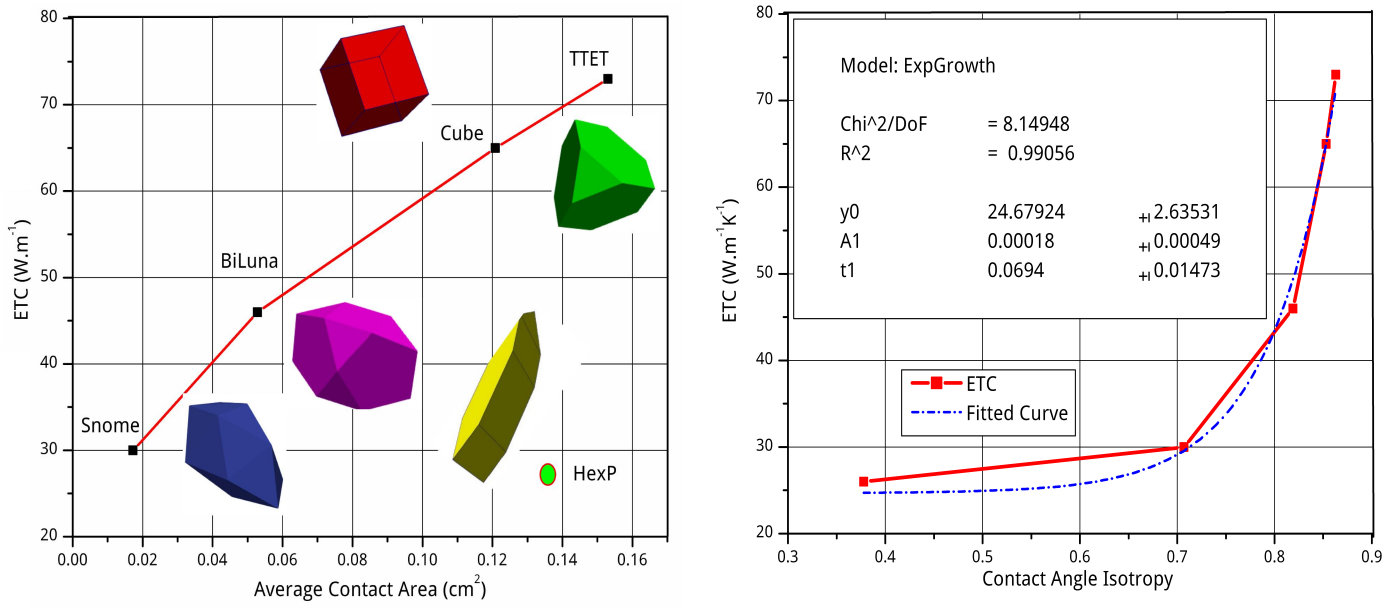

(a) (b)

Figure 14: Effective thermal conductivity for convex polyhedra as a function of (a) contact area and (b) contact angle isotropy.

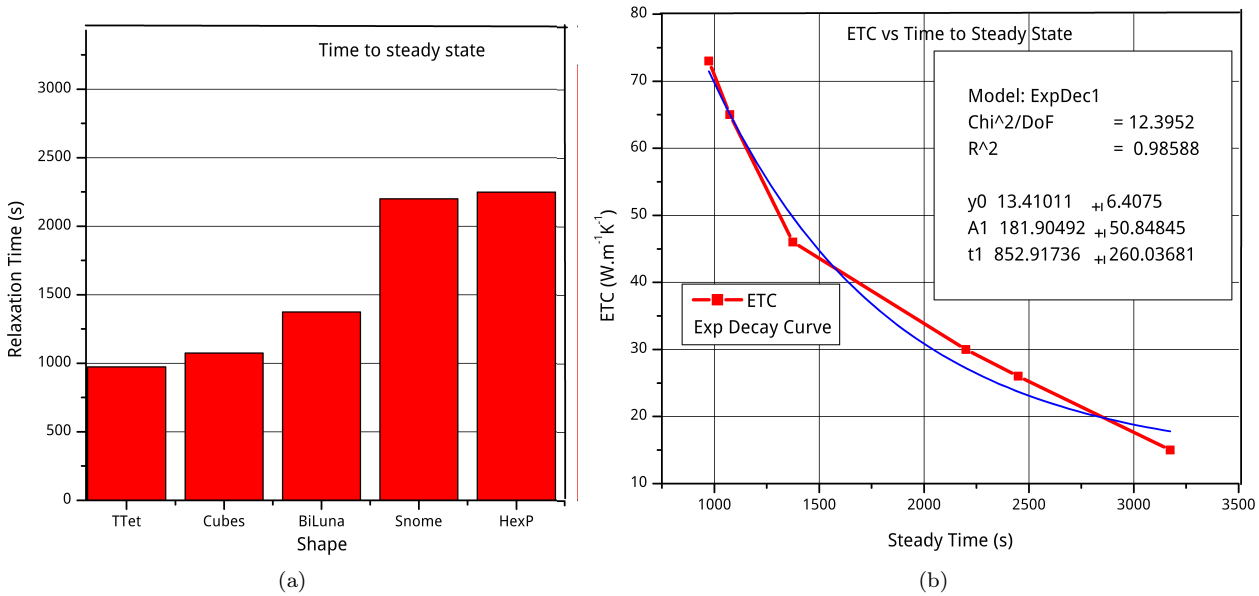

(a) (b)

Figure 15: (a) ETC as a function of the time to reach steady state and (b) time to reach steady state for the various shapes.

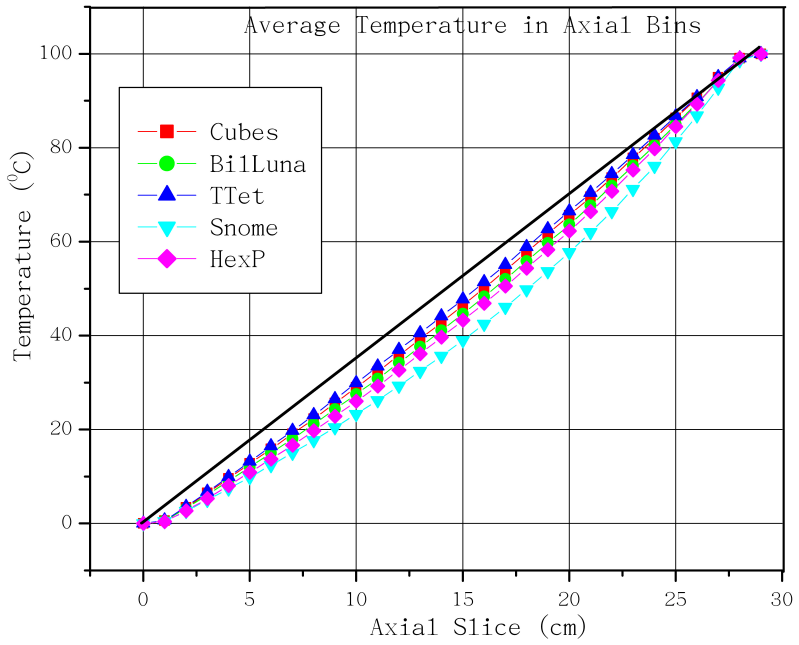

(a)

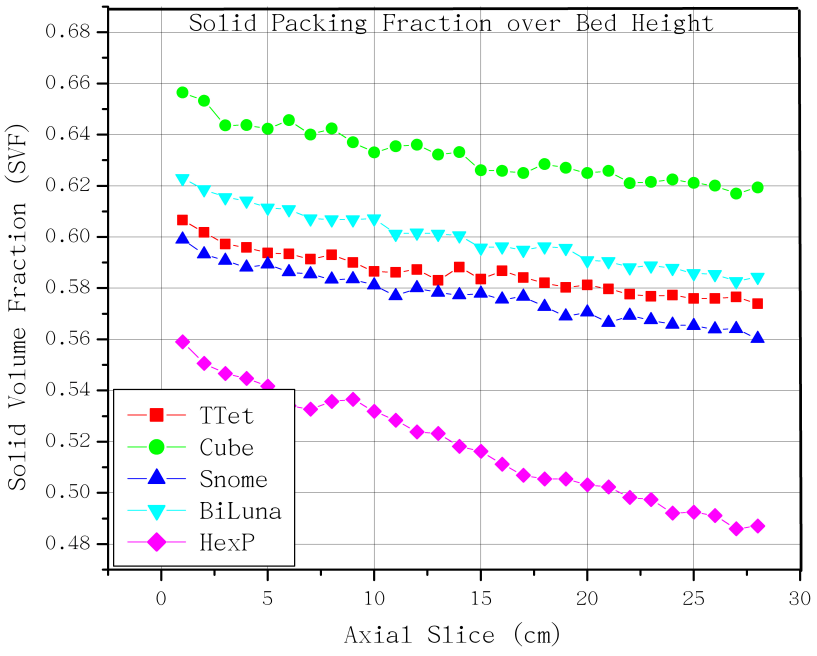

(b)

Figure 16: (a) Plot of average temperature and (b) solid packing fraction in vertical slices (1 cm)

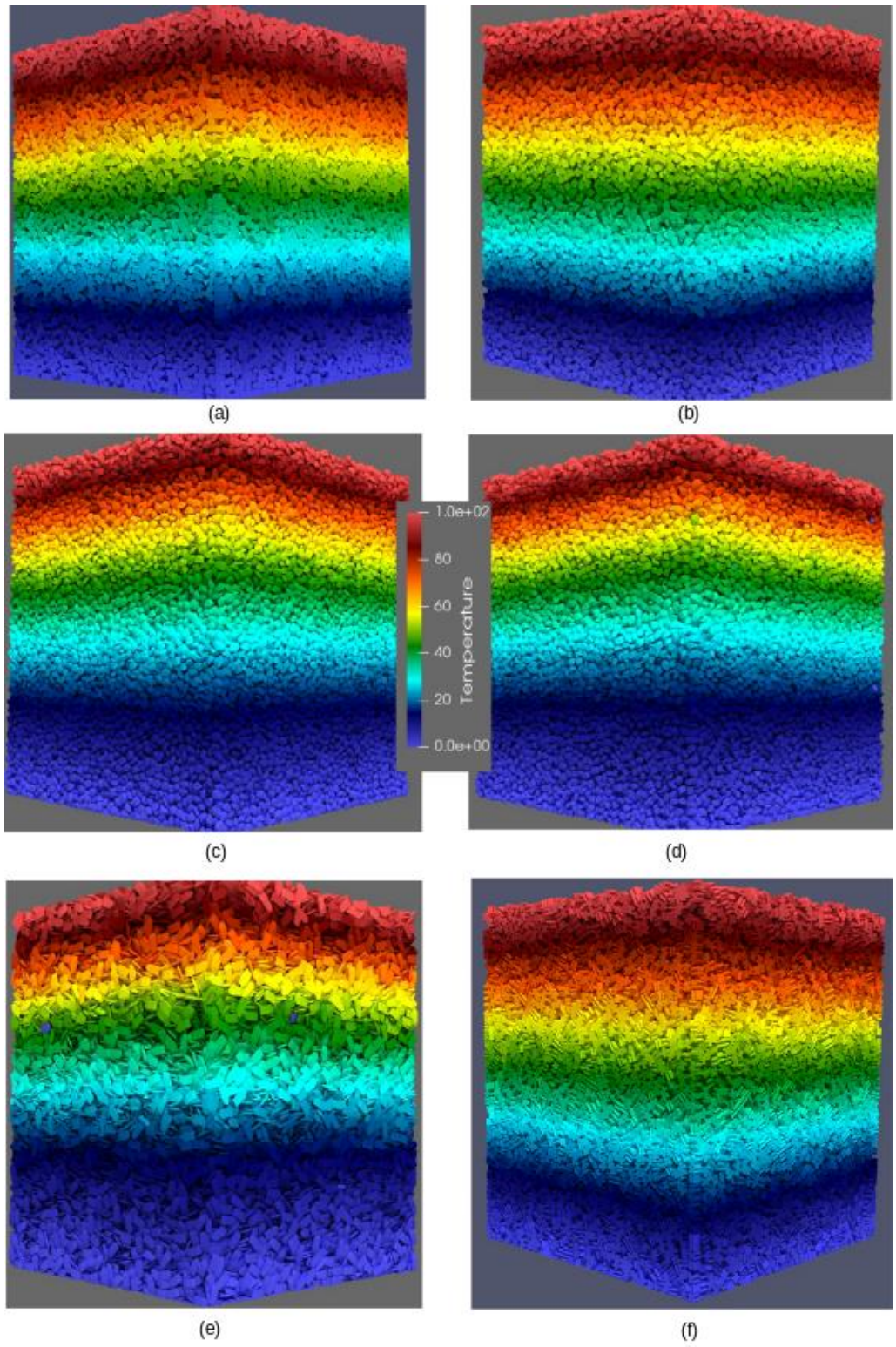

Figure 17: The temperature distribution comparison of (a) cubic, (b) truncated tetrahedron, (c) bilunabirotunda, (d) sphenomegacorona , (e) flattened augmented hexagonal prism particles.

Tables

Physical property	Notation	Value
particle density (kg.m^{-3})	ρ	2700
volume (cm^3)	V_p	0.125
friction coefficient	μ	0.40
normal stiffness (N.m^{-1})	K_n	4000
gravity acceleration (ms^{-2})	g	9.81
thermal conductivity ($\frac{W}{m.K}$)	λ_p	240
specific thermal capacity $\frac{J}{kg.K}$.	c_p	921
Poisson's ratio of particle	ν	0.32
restitution coefficient	e	0.45
time step (s)	$\triangle t$	1×10^{-5}

Table 1: Particle material properties.

Shape (Figure)	SA (cm^2)	#P	#Faces	#Edges	SVF	ETC ($\frac{w}{m.k}$)	Avg CArea	Isotropy
TTet (b)	1.5381	94,305	8	18	*0.5859*	*73*	*0.1530*	*0.8634*
Cube (a)	1.5003	92,706	6	12	*0.6351*	*65*	*0.1208*	*0.8537*
Biluna (c)	1.4445	90,831	14	26	*0.5986*	*46*	*0.0527*	*0.8191*
Sphenome (d)	1.4280	89,961	18	28	*0.5763*	*30*	*0.0172*	*0.7072*
HexP (e)	2.2863	81,517	11	22	*0.5373*	*26*	*0.1250*	*0.3784*
CrossP (f)	*3.384*	*102,136*	*16*	*36*	*0.6725*	*25*	*0.0049*	*0.9062*
Sphere (r=0.310)	*1.2109*	*96,858*	-	-	*0.6358*	*15*	*0.0047*	*1.0000*

Table 2: Particle shapes and packed bed ETCs.

References

[1] P. G. de Gennes. Granular matter: a tentative view. *Rev. Mod. Phys.*, 71:S374–S382, Mar 1999.

[2] Hong Hwee. Lee. Catalyst preparation by impregnation and activity distribution. 1984.

[3] V.D. Nguyen, C. Cogne, M. Guessasma, E. Bellenger, and J. Fortin. Discrete modeling of granular flow with thermal transfer: Application to the discharge of silos. *Applied Thermal Engineering*, 29(8):1846 – 1853, 2009.

[4] Bodhisattwa Chaudhuri, Fernando J. Muzzio, and M. Silvina Tomassone. Modeling of heat transfer in granular flow in rotating vessels. *Chemical Engineering Science*, 61(19):6348 – 6360, 2006.

[5] Bodhisattwa Chaudhuri, Fernando J. Muzzio, and M. Silvina Tomassone. Experimentally validated numerical modeling of heat transfer in granular flow in rotating vessels. In Aziz Belmiloudi, editor, *Heat Transfer*, chapter 12. IntechOpen, Rijeka, 2011.

[6] Peter J. Witt, Matthew D. Sinnott, Paul W. Cleary, and M. Philip Schwarz. A hierarchical simulation methodology for rotary kilns including granular flow and heat transfer. *Minerals Engineering*, 119:244 – 262, 2018.

[7] Aainaa Izyan Nafsun, Fabian A. D. Herz, Eckehard Specht, Hendrik Komossa, Siegmar Wirtz, and Viktor Scherer. Experimental investigation of thermal bed mixing in rotary drums. 2015.

[8] Jon T. Van Lew, Alice Chan Ying Ying, and Mohamed Aly Abdou. A discrete element method study on the evolution of thermomechanics of a pebble bed experiencing pebble failure. 2014.

[9] Amit Amritkar. Parallel implementation and application of particle scale heat transfer in the discrete element method. 2013.

[10] A.M. Scott and J. Bridgwater. Interparticle percolation: A fundamental solids mixing mechanism. *Ind. Eng. Chem. Fundamen.*, 14:22–27, 1975.

[11] S. N. Pathak, V. Esposito, A. Coniglio, and M.P. Ciamarra. Force percolation transition of jammed granular systems. *Physics Review E*, 86:042901, 2017.

[12] Ivan C. Christov, Julio M. Ottino, and Richard M. Lueptow. From streamline jumping to strange eigenmodes: Bridging the lagrangian and eulerian pictures of the kinematics of mixing in granular flows. *Physics of Fluids*, 23(10), 10 2011.

[13] P. K. Haff. Grain flow as a fluid-mechanical phenomenon. *Journal of Fluid Mechanics*, 134:401–430, 1983.

[14] D. V. Khakhar, Ashish V. Orpe, and J. M. Ottino. Continuum model of mixing and size segregation in a rotating cylinder: Concentration-flow coupling and streak formation. *Powder Technology*, 116(2-3):232–245, 5 2001.

[15] Steven W. Meier, Richard M. Lueptow, and Julio M. Ottino. A dynamical systems approach to mixing and segregation of granular materials in tumblers. *Advances in Physics*, 56(5):757–827, 2007.

[16] Watson L. Vargas and J. J. McCarthy. Thermal expansion effects and heat conduction in granular materials. *Phys. Rev. E*, 76:041301, Oct 2007.

[17] Gulad Kuuk, Marcial Gabino Marquez Gonzalez, and Alberto M. Cuitino. Effective thermal expansion property of consolidated granular materials. In *Materials*, 2017.

[18] Xiaoliang Wang, Jie Zheng, and Hongli Chen. Application of a model to investigate the effective thermal conductivity of randomly packed fusion pebble beds. *Fusion Engineering and Design*, 106:40 – 50, 2016.

[19] Yusuke Asakuma, Yushin Kanazawa, and Tsuyoshi Yamamoto. Thermal radiation analysis of packed bed by a homogenization method. *International Journal of Heat and Mass Transfer*, 73:97 – 102, 2014.

[20] Dorca Polamuri and Sunil Kumar Thamida. Experimental determination of effective thermal conductivity of granular material by using a cylindrical heat exchanger. *International Journal of Heat and Mass Transfer*, 81:767 – 773, 2015.

[21] Sakae Yagi and Daizo Kunii. Studies on effective thermal conductivities in packed beds. *AIChE Journal*, 3(3):373–381, 1957.

[22] V. V. R. Natarajan and M. L. Hunt. Heat transfer in vertical granular flows. *Experimental Heat Transfer*, 10(2):89–107, 1997.

[23] Jaona Randrianalisoa and Dominique Baillis. Radiative properties of densely packed spheres in semitransparent media: A new geometric optics approach. *Journal of Quantitative Spectroscopy and Radiative Transfer*, 111(10):1372 – 1388, 2010.

[24] G. Buonanno and A. Carotenuto. The effective thermal conductivity of a porous medium with interconnected particles. *International Journal of Heat and Mass Transfer*, 40(2):393 – 405, 1997.

[25] F. Huchet, Patrick Richard, Jules Joniot, and Leguen Lauredan. Heat transfer rate within non-spherical thick grains. *EPJ Web of Conferences*, 140:02015, 01 2017.

[26] Hongwei Zhang, Q. Zhou, and Yonggang Zheng. A multi-scale method for thermal conduction simulation in granular materials. *Computational Materials Science - COMPUT MATER SCI*, 50:2750–2758, 08 2011.

[27] Yusuke Asakuma, Masahiro Asada, Yushin Kanazawa, and Tsuyoshi Yamamoto. Thermal analysis with contact resistance of packed bed by a homogenization method. *Powder Technology*, 291:46 – 51, 2016.

[28] D. Mandal, D. Sathiyamoorthy, and M. Vinjamur. Void fraction and effective thermal conductivity of binary particulate bed. *Fusion Engineering and Design*, 88(4):216 – 225, 2013.

[29] Junghwoon Lee, Tae Sup Yun, and Sung-Uk Choi. The effect of particle size on thermal conduction in granular mixtures. *Materials*, 8:3975–3991, 2015.

[30] Cheng-An Wang, Lan-Xin Ma, Jian-Yu Tan, and Lin-Hua Liu. Study of radiative transfer in 1d densely packed bed layer containing absorbing-scattering spherical particles. *International Journal of Heat and Mass Transfer*, 102:669 – 678, 2016.

[31] Y.T. Feng, K. Han, C.F. Li, and D.R.J. Owen. Discrete thermal element modelling of heat conduction in particle systems: Basic formulations. *Journal of Computational Physics*, 227(10):5072 – 5089, 2008.

[32] E. S. Huetter, N. I. Koemle, G. Kargl, and E. Kaufmann. Determination of the effective thermal conductivity of granular materials under varying pressure conditions. *Journal of Geophysical Research: Planets*, 113(E12), 2008.

[33] Mehran Kiani-Oshtorjani and Payman Jalali. Thermal discrete element method for transient heat conduction in granular packing under compressive forces. *International Journal of Heat and Mass Transfer*, 145:118753, 2019.

[34] Anthony G. Dixon. Wall and particle-shape effects on heat transfer in packed beds. *Chemical Engineering Communications*, 71(1):217–237, 1988.

[35] Tae Sup Yun and T. Matthew Evans. Three-dimensional random network model for thermal conductivity in particulate materials. *Computers and Geotechnics*, 37(7):991 – 998, 2010.

[36] I. Terreros, I. Iordanoff, and J.L. Charles. Simulation of continuum heat conduction using dem domains. *Computational Materials Science*, 69:46 – 52, 2013.

[37] T. Oschmann, M. Schiemann, and H. Kruggel-Emden. Development and verification of a resolved 3d inner particle heat transfer model for the discrete element method (dem). *Powder Technology*, 291:392 – 407, 2016.

[38] Vinay V. Mahajan, Tim M.J. Nijssen, J. A.M. Kuipers, and Johan T. Padding. Non-spherical particles in a pseudo-2d fluidised bed: Modelling study. *Chemical Engineering Science*, 192:1105–1123, 8 2018.

[39] Q. Zhou, Hongawei Zhang, and Yonggang Zheng. A homogenization technique for heat transfer in periodic granular materials. *Advanced Powder Technology - ADVANCED POWDER TECHNOL*, 23, 01 2012.

[40] Marc G. D. Geers, Varvara G. Kouznetsova, Karel Matoua, and Julien Yvonnet. *Homogenization Methods and Multiscale Modeling: Nonlinear Problems*, pages 1–34. American Cancer Society, 2017.

[41] C. Wellmann and P. Wriggers. *Homogenization of Granular Material Modeled by a 3D DEM*, pages 211–231. Springer Netherlands, Dordrecht, 2011.

[42] P. Wriggers and J. Nettingsmeier. *Homogenization and Multi-Scale Approaches for Contact Problems*, pages 129–161. Springer Vienna, Vienna, 2007.

[43] Evan Mitsoulis and John Vlachopoulos. The finite element method for flow and heat transfer. *Advances in Polymer Technology*, 4:107 – 121, 06 1984.

[44] Artur Cebula and Dawid Taler. *Finite Volume Method in Heat Conduction*, pages 1645–1658. Springer Netherlands, Dordrecht, 2014.

[45] A. Mitchell and David Griffiths. *The Finite Difference Method in Partial Differential Equations*. 01 1980.

[46] H.W. Zhang, Q. Zhou, H.L. Xing, and H. Muhlhaus. A dem study on the effective thermal conductivity of granular assemblies. *Powder Technology*, 205(1):172 – 183, 2011.

[47] Ali Tarokh, Abdulmajeed Mohamad, and L. Jiang. Simulation of conjugate heat transfer using the lattice boltzmann method. *Numerical Heat Transfer Part A - Applications*, 63:159–178, 01 2013.

[48] Paul W Cleary and Joseph J Monaghan. Conduction modelling using smoothed particle hydrodynamics. *Journal of Computational Physics*, 148(1):227 – 264, 1999.

[49] Zarghaam Rizvi, Amir Shoarian Sattari, and Frank Wuttke. *Numerical analysis of heat conduction in granular geo-material using lattice element method*, pages 367–371. 08 2016.

[50] Yuanbo Liang and Xikui Li. A new model for heat transfer through the contact network of randomly packed granular material. *Applied Thermal Engineering*, 73(1):984 – 992, 2014.

[51] W. van Antwerpen, P.G. Rousseau, and C.G. du Toit. Multi-sphere unit cell model to calculate the effective thermal conductivity in packed pebble beds of mono-sized spheres. *Nuclear Engineering and Design*, 247:183 – 201, 2012.

[52] H. Haddad, M. Guessasma, and J. Fortin. Heat transfer by conduction using dem-fem coupling method. *Computational Materials Science*, 81:339 – 347, 2014.

[53] Clément Joulin, Jiansheng Xiang, John-Paul Latham, and Christopher Pain. A new finite discrete element approach for heat transfer in complex shaped multi bodied contact problems. In Xikui Li, Yuntian Feng, and Graham Mustoe, editors, *Proceedings of the 7th International Conference on Discrete Element Methods*, pages 311–327, Singapore, 2017. Springer Singapore.

[54] Chengzeng Yan and YuYong Jiao. FDEM-TH3D: a three-dimensional coupled hydrothermal model for fractured rock. *International Journal for Numerical and Analytical Methods in Geomechanics*, 43(1):415–440, 2019.

[55] N S Saxena, M Aslam Chohan, and S E Gustafsson. Effective thermal conductivity of loose granular materials. *Journal of Physics D: Applied Physics*, 19(9):1625–1630, sep 1986.

[56] David L. Swift. The thermal conductivity of spherical metal powders including the effect of an oxide coating. *International Journal of Heat and Mass Transfer*, 9(10):1061 – 1074, 1966.

[57] A. Nasirian, D. D. Cortes, and S. Dai. The physical nature of thermal conduction in dry granular media. *Geotechnique Letters*, 5(1):1–5, 2015.

[58] Pavel Grinchuk, S.M. Danilova-Tret'yak, and N.I. Stetyukevich. Force chains influence on the conductivity of granular media. *Doklady af the Natio?al ???d?m? of S?i????s of Belarus*, 57:105–112, 07 2018.

[59] Weijing Dai, Dorian Hanaor, and Yixiang Gan. The effects of packing structure on the effective thermal conductivity of granular media: A grain scale investigation. *International Journal of Thermal Sciences*, 142:266 – 279, 2019.

[60] Pooya Azadi, Ramin Farnood, and Ning Yan. Fem-dem modeling of thermal conductivity of porous pigmented coatings. *Computational Materials Science*, 49(2):392 – 399, 2010.

[61] Y T Feng, K Han, and D R J Owen. Energy-conserving contact interaction models for arbitrarily shaped discrete elements. *Computer Methods in Applied Mechanics and Engineering*, pages 169–177, 2012.

[62] M Pasha, C Hare, M Ghadiri, A Gunadi, and PM Piccione. Effect of particle shape on flow in discrete element method simulation of a rotary batch seed coater. *Powder Technology*, 296:29–36, August 2016. © 2015, Elsevier. This is an author produced version of a paper published in Powder Technology. Uploaded in accordance with the publisher's self-archiving policy.

[63] Hiroshi Mio, Toshiki Nakauchi, Yuuki Kawaguchi, Takashi Enaka, Yoichi Narita, Atsushi Inayoshi, Shinroku Matsukazi, Takashi Orimoto, and Seiji Nomura. High-speed video recording of particle trajectory via rotating chute of nagoya no.3 blast furnace and its comparison with simulated behavior using dem. *ISIJ International*, 57(2):272–278, 2017.

[64] Kamyar Kildashti, Kejun Dong, Bijan Samali, Qijun Zheng, and Aibing Yu. Evaluation of contact force models for discrete modelling of ellipsoidal particles. *Chemical Engineering Science*, 177:1 – 17, 2018.

[65] H. Abou-Chakra, J. Baxter, and U. Tuzun. Three-dimensional particle shape descriptors for computer simulation of non-spherical particulate assemblies. *Advanced Powder Technology*, 15:63–77, 2004.

[66] N. Govender, D. Wilke, S. Kok, and R. Els. Development of a convex polyhedral discrete element simulation framework for NVIDIA Kepler based GPUs. *Journal of Computational and Applied Mathematics*, 270:63–77, 2014.

[67] N. Govender, D. Wilke, and S. Kok. Collision detection of convex polyhedra on the NVIDIA GPU architecture for the discrete element method. *Applied Mathematics and Computation*, 267:810–829, 2015.

[68] Nicolin Govender, Daniel N. Wilke, Chuan-Yu Wu, Raj Rajamani, Johannes Khinast, and Benjamin J. Glasser. Large-scale gpu based dem modeling of mixing using irregularly shaped particles. *Advanced Powder Technology*, 29(10):2476 – 2490, 2018.

[69] B. Smeets, T. Odenthal, S. Vanmaercke, and H. Ramon. Polygon-based contact description for modeling arbitrary polyhedra in the Discrete Element Method. *Computer Methods in Applied Mechanics and Engineering*, 290:277–289, jun 2015.

[70] Victor Klee. Maximal Separation Theorems for Convex Sets. *Transactions of the American Mathematical Society*, 134(1):133–147, 1968.

[71] Helge Tverberg. A separation property of plane convex sets. *Mathematica Scandinavica*, 45(2):255–260, 1980.

[72] C.W. Boon, G.T. Houlsby, and S. Utili. A new algorithm for contact detection between convex polygonal and polyhedral particles in the discrete element method. *Computers and Geotechnics*, 44:73–82, jun 2012.

[73] Jan Elias. DEM simulation of railway ballast using polyhedral elemental shapes. In *III International Conference on Particle-based Methods Fundamentals and Applications*, pages 1–10, 2013.

[74] Nicolin Govender, Daniel N. Wilke, Chuan-Yu Wu, Ugur Tuzun, and Hermann Kureck. A numerical investigation into the effect of angular particle shape on blast furnace burden topography and percolation using a gpu solved discrete element model. *Chemical Engineering Science*, 204:9 – 26, 2019.